A Training System for Ultrasound-Guided Needle Insertion Procedures

Yanong Zhu[1], Derek Magee[1], Rish Ratnalingam[2], and David Kessel[3]

[1] School of Computing, University of Leeds, Leeds, UK
[2] Mid Yorkshire Hospitals NHS Trust, Wakefield, UK
[3] Leeds Teaching Hospitals NHS Trust, Leeds, UK

Abstract. Needle placement into a patient body under guidance of ultrasound is a frequently performed procedure in clinical practice. Safe and successful performance of such procedure requires a high level of spatial reasoning and hand-eye co-ordination skills, which must be developed through intensive practice. In this paper we present a training system designed to improve the skills of interventional radiology trainees in ultrasound-guided needle placement procedures. Key issues involved in the system include surface and volumetric registration, solid texture modelling, spatial calibration, and real-time synthesis and rendering of ultrasound images. Moreover, soft tissue deformation caused by the needle movement and needle cutting is realised using a mass-spring-model approach. These have led to a realistic ultrasound simulation system, which has been shown to be a useful tool for the training of needle insertion procedures. Preliminary results of a construct evaluation study indicate the effectiveness and usefulness of the developed training system.

1 Introduction

Needle placement into deep organs of a patient is a frequently performed interventional procedure, which may be carried out for a range of purposes, such as drainage of abscess, relief of blockages in the kidneys, radioactive seed implantation, and biopsy of deep tissues. Although usually guided by real-time ultrasound display, such procedures are still highly risky, and require a high level of spatial reasoning and hand-eye co-ordination skill, for successful performance and patient safety. The only reliable approach to acquisition of such professional skills is practicing in a specialised training regime. While practicing needle placement on human patients is dangerous and impractical, and the use of animals is inaccurate, an obvious solution is using simulation systems for the training of such interventional procedures.

Computerised surgical simulation is gaining extensive research interest among both medical and computing communities. Although major efforts have been devoted to simulation of minimally invasive surgery and open surgery involving large incisions, there is relatively limited development in the simulation of image-guided needle-based procedures [1]. Alterovitz *et al* [2] presented a program to simulate soft tissue deformation caused by needle movement. A single ultrasound image of the prostate is warped dynamically according to the deforming planar

N. Ayache, S. Ourselin, A. Maeder (Eds.): MICCAI 2007, Part I, LNCS 4791, pp. 566–574, 2007.

mass-spring mesh. A key limitation of this study is that no 3D aspects of the procedure is implemented. Gorman *et al* [3] developed a system incorporating a mannequin and a haptic feedback device for the simulation of lumbar puncture procedure, which is based on offline CT data. This has no real-time visual feedback. Simulators for fluoroscopy (2D X-ray based imaging) guided procedures have also been reported [4,5]. Nonetheless, ultrasound is often preferable for the guidance of such procedures, as it is fully real-time and inherently safe, while exposure to X-ray should be minimised. Forest *et al* [6] presented an ultrasound simulator named HORUS. Some ultrasould artifacts, such as absorbtion and echos, were implemented, however the general appearance of the simulated ultrasound images was mainly based on CT images, which are essentially different from ultrasound. Moreover, although haptic devices may provide the feeling of "touching" and interacting with the virtual models to some degree, operating on a physical model is a more direct and realistic simulation of the real scenario.

Our target is to develop an ultrasound simulation system that reproduces the ultrasound-guided needle insertion procedure as closely as possible, such that the skills acquired on the simulator can be transported to practical operations with little effort. The hardware of our simulator consists of three components, a standard PC (Dual Intel® Xeon™ CPU 3.20 GHz, 2.0 GB of RAM, running Microsoft® Windows® XP™ Professional), a full scale penetrable model made of latex, plastic and foam, and a pair of Ascension PCIBirds magnetic 3D position/orientation sensors. One of the sensors is rigidly attached to a mock ultrasound probe, and the other attached to a standard biopsy needle. The system process flowchart is shown in Figure 1. For conciseness, in the following sections we will only briefly describe the offline processes in stage i, ii and iii, and focus on the real-time processes such as image synthesis and deformation modelling. Algorithmic details for data registration, sensor calibration, and construction of texture bank, may be found in [7] and [8].

2 Methods

2.1 Offline Processes

The synthesis of virtual ultrasound images requires the answer to three questions: where is the ultrasound scan plane w.r.t. the body, what is in the image, and what does it look like. The position and orientation of the scan plane are captured by the motion sensor that is rigidly attached to the ultrasound probe. A calibration function from the sensor to the calibration point at the centre of the end of the probe is estimated from multiple unique position samples using a standard Least Square Fitting method. Similar approach can be applied to the probe direction calibration, as well as the needle calibration [7]. A volumetric CT data set, acquired from a live patient, is first manually labelled, and then aligned to the physical model surface using a quadratic warping function estimated by a two-stage surface registration process [7]. Sampling this warped volume in the scan plane yields the tissue type of each pixel in the image. The basic appearance of ultrasound imaging is determined by a set of volumetric textures (one for

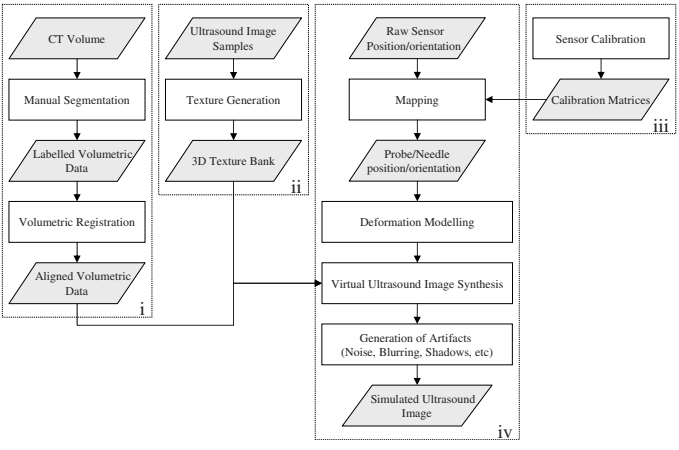

Fig. 1. Simulation process of ultrasound imaging

each visually distinct tissue type) that is synthesised from sets of selected 2D ultrasound examples [8].

2.2 Soft Tissue Deformation

Modelling of the deformation of soft tissue caused by the needle movement is essential for the simulation of ultrasound-guided needle placement as it increases the fidelity of the simulated process. More importantly, it provides immediate indication of needle location and orientation when the needle is invisible in the image but still reasonably close to the scan plane. On the other hand, however, we assume that a highly complex and accurate model for the deforming effect might be unnecessary in our case for two reasons, i) the deformation only needs to be accurate enough to indicate needle location and orientation, and ii) it must be simple enough to work in real-time.

Mass-spring and Finite Element methods are commonly applied methods in the domain of surgical simulation [9]. For the reason of computational efficiency and simplicity, we adopt a localised mass-spring model that is simplified to fit our problem. Firstly, all tissue types are assumed to have identical physical properties and interfaces between tissues are not considered. Although this would not allow the modelling of complex interactions, we have included some facilities that detect whether the needle hits bones or other crutial structures. Secondly, the needle is a thin and sharp device, and only causes deformation in the region local to the insertion path. Therefore, once the needle is detected to have broken the skin, a cylindrical deforming field centred at the predicted insertion path (i.e., the current direction of the needle) is created in the form of a tetrahedral mesh. Physical properties of the mesh elements, such as node mass, spring stiffness, and spring damping factor, are initialised using the methodology described in [10]. A reference mesh with identical topology, named $\hat{M}$, is created to represent

the static locations of the vertices, while the deformed mesh, M, represents the dynamic vertex positions according to the mass-spring model. Although the mass-spring method is simple in concept, and has standard solutions, two key issues must be solved in our application, as discussed below.

Mesh Manipulation. In a mass-spring model, external forces can only be applied to its nodes. It is important that, during needle insertion, a mesh node is always constrained at the tip, and all penetrated nodes are constrained to only move along the needle shaft. We use a first-in-last-out stack, $\boldsymbol{v}_{shaft}$, to store the shaft nodes, and use v_{tip} to denote the current tip-node. When v_{tip} is penetrated, it is pushed into the stack, and a new tip-node is identified and assigned to v_{tip}. Figure 2 (a) shows the initial status of $\boldsymbol{v}_{shaft}$ and v_{tip} at a time point t, as well as the tetrahedron defined by $\{v_{j0}, v_{j1}, v_{j2}, v_{j3}\}$ that will enclose the needle tip at time $t+1$. Let v_{j0} be the current tip-node ($v_{tip} = v_{j0}$), P_{tip} be the new tip position at time $t+1$, and P_{inter} be the intersection point of the new needle direction with the triangle defined by $\{v_{j1}, v_{j2}, v_{j3}\}$. We consider v_{tip} as penetrated if $distance(P_{inter}, P_{tip}) \leq \lambda \cdot circumference(v_{j1}, v_{j2}, v_{j3})$, where λ is a constant that controls how much the tip node may be displaced before it is penetrated (empirically selected as 0.05 in our current model). The use of circumference ensures this criterion is invariant to the size of the enclosing tetrahedron. When the criterion is satisfied, the tip node is appended to $\boldsymbol{v}_{shaft}$, and v_{tip} is set to be empty. The mass-spring system is then advanced by one time step to $t+1$ (see Figure 2 (b)). Subsequently, the closest of v_{j1}, v_{j2} and v_{j3} to P_{inter} is moved to P_{tip} and assigned as the new tip-node v_{tip} (v_{j3} in the example in Figure 2 (c)).

Moving a node to a new position in the mesh requires two sub-steps. Firstly, the corresponding node in the reference mesh must be moved accordingly. This is solved by using the Barycentric coordinates, which allow us to map an arbitrary point in the deformed mesh to its corresponding position in the reference mesh, or vice versa. Let $\boldsymbol{b} = \{b_0, b_1, b_2, b_3\}$ be the Barycentric coordinates of point P within the i^{th} tetrahedron, T_i, i.e., $P = \boldsymbol{b}\boldsymbol{v}'_i$, where $\boldsymbol{v}_i = \{v_{i0}, v_{i1}, v_{i2}, v_{i3}\}$ are the vertices of T_i. The corresponding position of P in $\hat{M}$, $\hat{P}$, is thus given by $\hat{P} = \boldsymbol{b}\hat{\boldsymbol{v}}'_i$. Secondly, physical properties of affected nodes/springs must be re-computed (see [10]). Since we maintain the lists of neighbouring nodes and connecting edges/tetrahedrons for all the mesh nodes, this can be done efficiently by iterating through the immediate neighbours of the moved node.

During needle retracking, there is no need to maintain a node at the needle tip. Hence we simply set v_{tip} to empty, and ordinally pop out the nodes in $\boldsymbol{v}_{shaft}$, as they come off the needle. To avoid oscillations after large movement of the needle, we linearly sub-sample the needle movements to ensure each step of movement is below a maximum length. This also ensures that the new tip node can be correctly identified even if the needle penetrates more than one tetrahedron in one time step.

Image Warping. Given the reference and deformed meshes at time t, the warped image can be produced by mapping each image pixel from the deformed

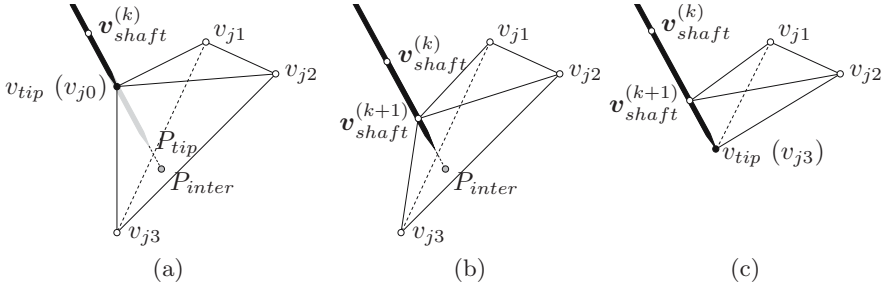

Fig. 2. Mesh manipulation for needle insertion in one step. The new position of the needle is shown in light grey, and current position in solid dark.

mesh to the reference mesh. It is safe to assume that, over a short period of time, most pixels will remain in the same tetrahedron as in the last frame, or appear in one of its neighbours due to mesh deformation. Thus we adopt a nearest-first strategy to perform efficient search of the appropriate tetrahedron for the computation of Barycentric coordinates. At the time when the mesh is first created, we search through the mesh to find the containing tetrahedron for every pixel. In later time steps, the search starts from the tetrahedron associated with the pixel in the previous frame, and propagates to its neighbours if necessary. This strategy greatly speeds up the mapping of coordinates between both meshes, which enables us to produce warped images in real-time.

2.3 Modelling the Needle

Apart from the deformation caused by the needle movement, the needle itself needs some specific handling. Since the motion sensor is fixed at the needle handle, the measured needle direction and tip position may be badly biased if the operator tries to adjust the needle direction by bending the needle. A bending constraining method is designed to minimise the measurement error, and approximate the location of the needle when it is bended within the body. Let $\mathbf{d}_m$ and $\mathbf{d_e}$ be the measured and entry direction of the needle, the constrained needle direction, $\mathbf{d}_c$, is given by $\mathbf{d}_c = w \cdot \mathbf{d}_e + (1 - w) \cdot \mathbf{d}_m$. The weight, w, is defined as $w = w_{max}/[1 + e^{-\alpha(l-\delta)}]$, where l is the inserted length of the needle shaft, w_{max} is the maximum value of weight, α defines the speed (smoothness) of transition from unconstrained to highly constrained bending as the needle is pushed forward, and δ controls the minimum needle length where the transition occurs (we currently use $w_{max} = 0.9$, $\alpha = 60$ and $\delta = 0.12$, based on extensive experiments and communication with our collaborating radiologists). To achieve realistic rendering of the needle, the ultrasound scan plane is assigned a thickness, t, and the brightness(visibility) of the needle shaft is determined by the intersection volume of the needle with the thickened scan plane. A value of t that is equal to the needle diameter appears to be appropriate in our simulator.

2.4 Simulation of Ultrasound-Specific Artifacts

Synthetic ultrasound images are generated by raster scanning through the pixels in the ultrasound portion of the scan plane. A number of imaging/graphic techniques are used to simulate ultrasound-specific artifacts and generate more realistic ultrasound images, as described in [8]. The speckle effect can be simply simulated by adding Gaussian distributed artificial noise to the image pixels. Shadows, caused by bones, air, and the needle shaft, are produced by a 2D ray-casting approach. The radial blur effect creates blurs around a specific point in an image, simulating the effects of a swirling camera. This is applied to simulate the radial scanning motion of a real ultrasound transducer.

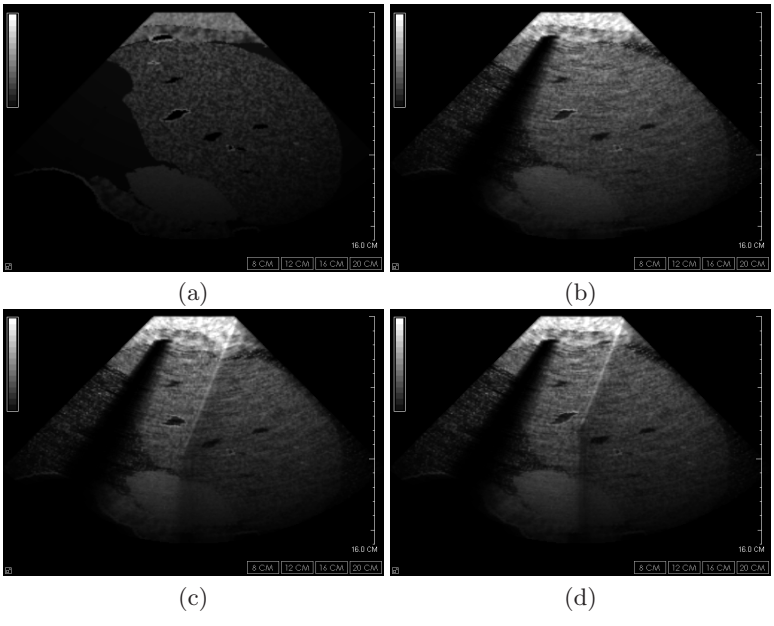

(a) (b)

(c) (d)

Fig. 3. Examples of synthetic ultrasound images. These images are slightly brightened for better display.

3 Results and Evaluation

Examples of simulated ultrasound images are shown in Figure 3. These include a "raw" synthetic ultrasound image constructed from the solid texture bank (Figure 3 (a)), and the final rendering results of the same image after artifact simulation (Figure 3 (b)). With the simulated features of speckle noise, blurring and shadowing, the improvement of realism is clear. The deformation due to needle movements may be better demonstrated dynamically. Figure 3 (c) and (d) illustrate the tissue deformation effect caused needle insertion and retracking, which is presented by the directional distortion of nearby structures.

Table 1. Definition of metrics

Principles	Metrics
The needle should not deviate from the optimal path (the straight line from entry point to the target).	m_1: Mean distance from needle tip to optimal path m_2: Mean angle from needle to optimal path
The needle should not deviate from the scan plane.	m_3: Mean distance from needle tip to scan plane m_4: Mean angle from needle to scan plane
The ultrasound probe should not move significantly after needle insertion	m_5: Mean angle from scan plane to entry plane
The needle should not be bended significantly	m_6: Mean distance from measured needle tip to constrained tip position. m_7: Mean angle from measured needle direction to constrained needle direction
The target should be visible in the image while the needle is inserted	m_8: Percentage of time when the target is visible m_9: Distance from target to scan plane
Needle tip should be close to the target.	m_{10}: Min distance from needle tip to target

A construct validation study of our simulation system as a training tool for ultrasound-guided needle insertion procedures is currently underway. The aim of the study is two-fold. On one hand, we hope to validate the realism of our system by showing that experienced experts are able to present superior performance on the simulator than novices as they are expected in real operation procedures. On the other hand, unskilled novices are predicted to perform less favourably due to the lack of practical experience, which may indicate the possibility to acquire and improve their skills through practicing on the simulation system.

We compare the performance of three groups of potential users of our system, including consultant radiologists, radiology registrars, and medical students. Each group consists of eight individuals. None of these twenty-four individuals has previous experience of our simulation system. The task for needle insertion is to find the target embedded in the liver, and hit it with a needle. Each individual is requested to perform three sessions with different target positions. Thus twenty-four sessions are recorded for each group.

Table 2. Performance comparison of three groups of users. All distances are in inches, and all angles are in radians. ($-^*$: $p < 0.05$, $-^{**}$: $p < 0.01$)

Metrics	Students	Registrars	Consultants	p-value (unpaired one-tail t-test)		
				Reg.vs.Stu	Con.vs.Stu	Con.vs.Reg
m_1	0.540 ± 0.122	0.541 ± 0.322	0.356 ± 0.045	0.5021	0.0160^*	0.0702
m_2	0.258 ± 0.035	0.255 ± 0.040	0.170 ± 0.004	0.4826	0.0179^*	0.0272^*
m_3	0.282 ± 0.032	0.259 ± 0.086	0.221 ± 0.018	0.3717	0.0943	0.2827
m_4	0.152 ± 0.015	0.095 ± 0.007	0.070 ± 0.002	0.0344^*	0.0015^{**}	0.0999
m_5	0.066 ± 0.005	0.051 ± 0.002	0.054 ± 0.003	0.1906	0.2455	0.5756
m_6	0.088 ± 0.008	0.094 ± 0.003	0.055 ± 0.001	0.6093	0.0487^*	0.0035^{**}
m_7	0.041 ± 0.000	0.034 ± 0.000	0.025 ± 0.000	0.1256	0.0011^{**}	0.0190^*
m_8	0.927 ± 0.023	0.978 ± 0.005	0.999 ± 0.000	0.0726	0.0123^*	0.0788
m_9	0.406 ± 0.049	0.388 ± 0.037	0.289 ± 0.023	0.3800	0.0194^*	0.0281^*
m_{10}	0.969 ± 0.967	0.635 ± 0.284	0.523 ± 0.102	0.0752	0.0200^*	0.1909

A set of quantitive metrics, based on the essential principles for the procedure, are designed to quantify the performance of different groups. What we are most concerned in each session is the period from when the needle breaks the skin till it leaves the body. Therefore, all these metrics are defined over this period, as listed in Table 1. Comparison of the measured performance is presented in Table 2 for all three groups. The group of consultants, who have extensive practical experience in such procedures, performed significantly better than the medical students ($p < 0.05$ for 8 of 10 metrics). Also, though to a less significant level, the superiority of consultants over registrars can also be observed ($p < 0.05$ for 4 of 10 metrics). Registrars performed slightly better than medical students, but not significantly. During the experiments, we noticed that the consultants usually try to identify the optimal path by varying the needle direction when the needle just breaks the skin, then maintain a nice straight line once the path is determined. This is believed to account for the observation that, for some of the metrics (e.g., $m1$ and $m3$), although the consultants presented better performance than other groups, the absolute measurements are not optimal.

4 Discussion

We have presented a ultrasound simulation system for the training of ultrasound guided needle insertion procedures. A number of computational techniques are involved, covering data registration, solid texture modelling, mass-spring modelling, and image processing. All of these are devoted to the development of a useful training system based on realistic simulation of real-time ultrasound imaging. Apart from the visual appearance of simulated images, the fidelity and validity of the system are further demonstrated by the results of construct validation study. It is non-trivial to implement haptic feedback in the system, since a physical latex model is used. However, highly realistic modelling of haptic feedback is seen to be less essential given that the system is designed to improve spatial reasoning and hand-eye co-ordination abilities. Major focuses of future work will include a longitudinal evaluation study that traces the performance of a group of trainees during a structured training course, and the development of a virtual "self-deforming" model of the human body that simulates the motions of the internal anatomies (e.g., respiration).

References

1. Liu, A., Tendick, F., Cleary, K., Kaufmann, C.: A survey of surgical simulation: applications, technology, and education. Presence: Teleoper. Virtual Environ. 12, 599–614 (2003)
2. Alterovitz, R., Pouliot, J., Taschereau, R., Hsu, I., Goldberg, K.: Simulating needle insertion and radioactive seed implantation for prostate brachytherapy. In: Proc. of MMVR, pp. 19–25 (2003)
3. Gorman, P., Krummel, T., Webster, R., Smith, M., Hutchens, D.: A prototype haptic lumbar puncture simulator. In: Proc. MMVR, pp. 106–109 (2000)

4. Li, Z., Chui, C., Anderson, J., Chen, X., Ma, X., Huai, W., Peng, Q., Cai, Y., Wang, Y., Nowinski, W.: Computer environment for interventional neuroradiology procedures. Simulation and Gaming 32, 405–420 (2001)
5. Vidal, F.P., John, N.W., Cuillemot, R.M.: Interactive physically-based x-ray simulation: CPU or GPU? In: Proc. of MMVR, pp. 479–481 (2007)
6. Forest, C., Comas, O., Vaysière, C., Soler, L., Marescaux, J.: Ultrasound and needle insertion simulators built on real patient-based data. In: Proc. of MMVR, pp. 136–139 (2007)
7. Magee, D., Kessel, D.: A computer based simulator for ultrasound guided needle insertion procedures. In: Proc. IEE International Conference on Visual Information Engineering, pp. 301–308 (2005)
8. Zhu, Y., Magee, D., Ratnalingam, R., Kessel, D.: A virtual ultrasound imaging system for the simulation of ultrasound-guided needle insertion procedures. In: Proc. of Medical Image Understanding and Analysis (2006)
9. Delingette, H., Ayache, N.: Surgery simulation and soft tissue modeling. In: Ayache, N., Delingette, H. (eds.) IS4TM 2003. LNCS, vol. 2673, pp. 12–13. Springer, Heidelberg (2003)
10. Paloc, C., Bello, F., Kitney, R., Darzi, A.: Online multiresolution volumetric mass spring model for real time soft tissue deformation. In: Dohi, T., Kikinis, R. (eds.) MICCAI 2002. LNCS, vol. 2489, pp. 219–226. Springer, Heidelberg (2002)